Article

Journal of
Nanoscience and Nanotechnology
Vol. 17, 1674–1680, 2017
www.aspbs.com/jnn

Synthesis and Characterization of Bulk Nanostructured Thermoelectric $Ca_3Co_4O_9$

A. Soffientini[1,*], I. G. Tredici[1], S. Boldrini[2], A. Famengo[2], G. Spinolo[1], and U. Anselmi-Tamburini[1]

[1] Department of Chemistry, University of Pavia, Viale Taramelli 12, I27100 Pavia, Italy
[2] CNR–IENI, Corso Stati Uniti 4, 35127 Padova, Italy

Nanostructuring has been proposed as an effective strategy for the reduction of the phonon contribution to the thermal conductivity, resulting in an increase in the figure of merit of thermoelectric materials. However, obtaining bulk samples presenting high relative density and nanometric grain size can be quite challenging, particularly in the case of ceramic phases. Only few examples have been reported and none in the case of $Ca_3Co_4O_9$. In this work, we used a sol–gel synthesis coupled with ball milling to prepare powders of $Ca_3Co_4O_9$ presenting a grain size as small as 4 nm. These nanopowders were then sintered at different temperature and pressures using the High-Pressure Field-Assisted Sintering Technique (HP-FAST). Relative densities up to 95 vol% where obtained while maintaining a nanometric grain size. The microstructural and electrical properties of the sintered samples have been characterized. The results show that in this oxide a reduction to the nanometric grain size produces a drastic reduction in the electrical conductivity, which cannot be compensated by the reduction in the thermal conductivity. The Seebeck effect, on the other hand, appears to be affected only marginally by the grain size and porosity.

Keywords: Thermoelectricity, Oxides, Cobaltites, Nanostructure, Sintering, HP-FAST.

1. INTRODUCTION

Thermoelectric (TE) materials can convert a thermal gradient into an electric potential through the Seebeck effect.[1] The conversion efficiency is expressed by an a dimensional figure of merit, $ZT = S^2\sigma T/(\kappa_{el} + \kappa_{ph})$, where S is the Seebeck coefficient, σ is the electrical conductivity, $\kappa_{el} + \kappa_{ph}$ the electron and phonon contribution to the thermal conductivity and T the absolute temperature. To achieve the best performance, a thermoelectric material requires a high power factor ($PF = S^2\sigma$) and a low thermal conductivity. However, S, σ and κ are related to each other, and the independent optimization of these parameters can be quite challenging. The best thermoelectric efficiency has been so far achieved using antimony, bismuth-, tellurium- and lead-based intermetallic compounds such as Bi_2Te_3, PbTe and $CoSb_3$, which can express a figure of merit above 1.[2–4] However, these materials present a high cost, high environmental toxicity and relatively low melting point, which limits their large scale and high temperature application. On the contrary, despite their low thermoelectric efficiency, oxides such as layered cobaltites, titanates or transition metal oxides[5] can be a valid alternative for high temperature applications, as they present low toxicity, low cost and elevated chemical resistance. Among these oxides, *p*-type calcium cobaltite $Ca_3Co_4O_9$ (referred also as CCO or C-349), has attracted particular interest.[6] In fact, it presents an electrical conductivity higher than 10^4 S/m, a Seebeck coefficient close to 200 μV/K and a thermal conductivity of around 2 W/m · K.[7] The low thermal conductivity derives mainly from the unusual crystallographic structure, presenting a monoclinic superlattice composed by two alternate layers, a conductive CdI_2-type hexagonal CoO_2 layer and a Ca_2CoO_3 rock-salt-type layer. These two sub-lattices share the same a, c and β lattice parameter, but differ in the b length, creating an incommensurate misfit.[8] The high electrical conductivity, on the other hand, is associated to the presence of CoO_2 layers that provide a preferential pathway for the charge carriers. For this reason texturing is often used to improve the performances of this material.[9]

*Author to whom correspondence should be addressed.

 1533-4880/2017/17/1674/007 doi:10.1166/jnn.2017.13729

Nanostructuring has been proposed as an effective strategy for obtaining an increase in the figure of merit of thermoelectric materials through the reduction of their thermal conductivity.[10] This approach, however, presents some drawbacks, as the electrical conductivity can be negatively affected as well. Aim of this work is to investigate how the nanostructure can influence the overall electrical properties of $Ca_3Co_4O_9$ bulk ceramics. Maintaining the nanostructure during the sintering process can be challenging in these materials, due to their rapid grain growth. In fact, no example of real bulk, sintered material preserving a nanometric grain size has been so far presented in the literature. In order to achieve this goal, the calcium cobaltite has been prepared by a simple sol–gel method, followed by a mild ball milling treatment. The sintering has been performed at different temperatures and pressures using a High-pressure Field-Assisted Sintering technique (HP-FAST), in order to obtain various grain sizes and relative densities. Then, thermoelectric properties have been measured and compared with calcium cobaltite with sub-micrometric grain size.

2. EXPERIMENTAL DETAILS

The $Ca_3Co_4O_9$ powder was prepared using a simplified sol–gel Pechini synthesis. In order to obtain 3 g of product, stoichiometric quantities of $Ca(NO_3)_2 \cdot 4H_2O$ and $Co(NO_3)_2 \cdot 6H_2O$ were dissolved into 130 ml of a solution of citric acid and distilled water with a citric acid-to-cations molar ratio of 1.3.[11] The clear pink solution was then heated under magnetic stirring at 100 °C overnight. The resulting dark pink gel was than dried at 120 °C for 2 h, ground and finally calcined following two different calcination methods, in order to obtain powders characterized by two different grain sizes. The first method (hereafter referred as method A) consisted in the direct calcination at 800 °C for 2 h, while in the second method (hereafter referred as method B) the precursor was first heated at 400 °C for 1 h, in order to remove the organic matrix, and then calcined at 700 °C for 2 h. The first method produced a sub-micrometric grain size (over 200 nm), while the second produced a nanometric (∼75 nm) powder. In order to reduce the grain size even further, the $Ca_3Co_4O_9$ powders obtained with method A have been ball milled using a planetary mill (Fritsch Pulverisette 7 Premium), tungsten carbide jars and 5 mm-diameter tungsten carbide balls, with a ball-to-powder mass ratio of 20:1. The milling process has been performed only on powders obtained using the method A, because preliminary investigations have shown no significant differences between milled samples deriving from powders obtained using method A and B. Two different milling speeds have been used: 400 rpm and 600 rpm, for a time of 4 h, divided into eight steps of 30 min. This procedure has been optimized in order to reduce powders inhomogeneity deriving from adhesion of the powders to jar walls.

All the $Ca_3Co_4O_9$ powders were finally sintered using a home-made High-Pressure Field-Assisted Sintering (HP-FAST) apparatus. Thanks to the application of high pressures and fast heating cycles, this technique allows to obtain the densification of the $Ca_3Co_4O_9$ powder using lower temperatures and much shorter times than in traditional sintering processes.[12] The use of this technique is crucial in order to obtain bulk materials maintaining nanometric grain size. In general, unmilled A powders have been used for obtaining sintered samples presenting a large grain size (>200 nm), B powder for obtaining sintered samples presenting an intermediate grain size (around 80 nm), while milled A powders have been used for obtaining sintered samples presenting the smallest grain size. The proper amount of powder was placed into a graphite die with silicon carbide plungers. After evacuation to a pressure of 10 Pa, the sample was heated at 200 °C/min up to the selected temperature and kept for 5 min under different uniaxial pressures and finally rapidly cooled down.

The sub-micrometric and the nanometric $Ca_3Co_4O_9$ powders have been sintered in a 10 mm die using several different temperatures and pressures up to 180 MPa (Table I). At the end of the sintering cycle some samples presented a superficial brown film composed of CoO and CaO, which was removed by grinding. The milled powders have been sintered at lower temperatures in order to avoid massive recrystallization and grain growth (Table II). In this case smaller samples have been produced (5 mm in diameter) using pressures up to 432 MPa. Relative densities over 90 vol% have been obtained.

X-ray diffraction patterns were obtained with a Bruker D8 ADVANCE diffractometer in Bragg-Brentano configuration and using a Cu Kα radiation for both powders and sintered samples. In the case of powders, a zero-background sample holder was used. In the case of sintered samples, the XRD have been taken on the surface parallel to the plane of compression, after removing at least 1 mm of sample using grinding paper. The sample crystallite size has been determined using the Scherrer formula:

$$\langle d \rangle = \frac{k\lambda}{\beta \cos\theta}$$

where d is the grain size k is a constant equal to 0.89, λ is the radiation wavelength, β is the FWHM and θ is the Bragg angle.

Table I. Sintering conditions for $Ca_3Co_4O_9$ samples used for thermoelectric characterizations prepared from sub-micrometric (A) and nanometric (B) powders.

Sample	T (°C)	P (MPa)	$\langle d \rangle$ (nm)	d%
S07A	800	108	>200	94
S08A	550	108	>200	70
S08B	550	108	80	66

Table II. Sintering conditions for $Ca_3Co_4O_9$ samples used for thermoelectric characterizations prepared from milled powders.

Sample	T (°C)	P (MPa)	$\langle d \rangle$ (nm)	d%
S09A	400	180	6	76
S24A	550	432	17	98
S25A	450	108	6	70

For the characterization of the electrical properties the sintered samples were cut into bars. The electrical conductivity was measured with a four-probe cell using a MaterialMates mod. 7260 Frequency Response Analyzer. The two sense electrodes were spaced by 2 mm. The Seebeck coefficient was measured using a home-made apparatus and determined from the slope of the $\Delta V/\Delta T$ plots.

The thermal diffusivity was measured by a laser flash thermal diffusivity apparatus (Netzsch LFA 457 MicroFlash) from RT to 800 °C in argon atmosphere (100 ml/min) on round pellets (diameter ≈ 12.7 mm) with a thickness of about 2 mm or 3 mm. The thermal conductivity κ was calculated according to the formula $\kappa = d\rho C_p$, where d (mm^2/s) is the thermal diffusivity, ρ (g/cm^3) is the geometrical density, and C_p (J/gK) is the specific heat. The specific heat was calculated using Netzsch Proteus analysis software by comparison with samples of a standard ceramic material with known C_p (Netzsch Pyroceram 9606). The declared relative uncertainty was 3% for diffusivity, 5% for specific heat and 7% for thermal conductivity.

The relative density of the samples was measured with the Archimedes' method considering a theoretical $Ca_3Co_4O_9$ density of 4.677 g/cm^3.[13]

The SEM micrographs were taken using a Tescan Mira3 HR-SEM, with an accelerating voltage of 20 kV.

3. RESULTS AND DISCUSSION

3.1. Synthesis

Figure 1 shows the XRD pattern of the $Ca_3Co_4O_9$ powders obtained after calcination with method A and B. The patterns show the presence of only one phase, corresponding to the compound $Ca_3Co_4O_9$ with no evidence of any secondary phases.[14] These patterns evidence also a strongly anisotropic microstructure. Large differences between the FWHM (Full Width at Half Maximum) of the various peaks are indeed observed. This is particularly evident in the pattern of the powder obtained with the method B (Fig. 1(B)). It can be noted as some peaks, particularly the ones corresponding to the 00il planes, appear to be quite sharp, while others, as the 1011, appear to be very broad (see Table III). The definition of an average grain size is very difficult in this situation. For this reason, we choose throughout the paper to report as sample grain size the value obtained using the peak 0020. This represents the maximum grain size, corresponding to a direction parallel to the basal planes of the lamellae. The dimension

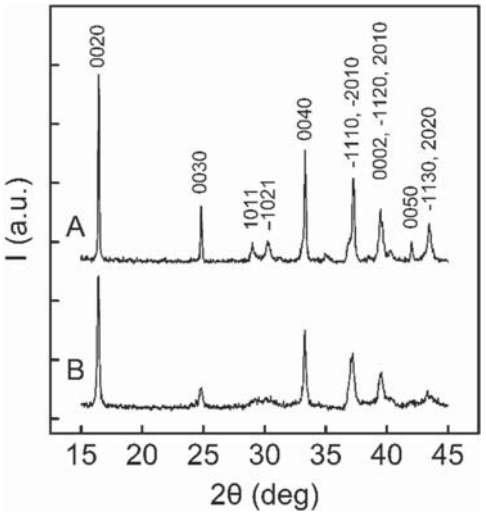

Figure 1. XRD pattern of $Ca_3Co_4O_9$ powder calcined with method A and method B. Peaks are indexed according to Ref. [8].

perpendicular to that direction would be in any case considerably smaller. The lamellar *habitus* of these powders is confirmed by the SEM images of Figure 2(a).

Figure 3 reports the XRD patterns of the CCO powders obtained using the method A after milling at 400 and 600 rpm for different times. It can be seen as even using these moderate milling conditions a drastic change in the material microstructure and crystallinity is produced. With a milling speed of 400 rpm the grain size is reduced from the sub-micrometric range to about 34 nm after the first hour of treatment, while the intensity of the peaks is strongly reduced, indicating a considerable level of amorphization. After 3 h even the strongest peaks disappear, leaving only broad bands. Using these residual peaks, a grain size of 4 nm can be estimated from the FWHM of the 0020 peak. Increasing the milling time to 4 h does not produce any further modification. The trend in the grain size and peak intensity relative to the 0020 peak, is reported in Figure 4. Increasing the milling speed to 600 rpm allows obtaining the almost complete amorphization within the first hour of treatment; a result that can be considered equivalent to the one obtained milling at 400 rpm for 3 hours. The 400 rpm/3 h condition was selected as the standard procedure. No further change is observed increasing the duration of the treatment.

Table III. XRD grain size calculated on the basis of different XRD peaks FWHM for $Ca_3Co_4O_9$ powder calcined with method B.

Peak	2θ (deg)	Calculated grain size (nm)
0020	16.4	77
0030	24.8	36
1011	29.1	14
−1021	30.2	6
0040	33.3	61

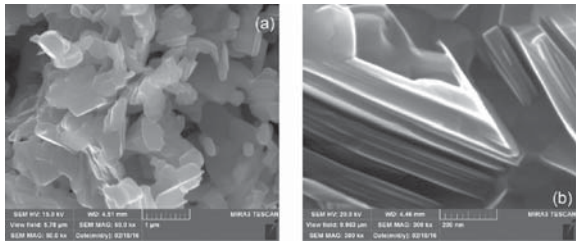

Figure 2. SEM micrograph of sub-micrometric $Ca_3Co_4O_9$ powder from method A (a) and the corresponding sintered sample S07A (b). The lamellar habitus of the particles is emphasized by the sintering process.

The morphology of these powders is shown in the SEM micrographs and reported in Figure 5(a). The milling treatment not only reduces the grain size, but also modifies the *habitus* of the grains. The grains, in fact, are no longer lamellar and appear to be composed by agglomerates of nanometric particles, not resolved in the reported image.

3.2. Sintering

In Figure 6 is reported the variation of temperature, pressure and sample thickness during a typical HP-FAST process, performed in this case on sub-micrometric powder (obtained from method A) at 800 °C. Evidences of densification are observed during the heating ramp, starting from temperatures just above 500 °C for sub-micrometric powders, while for the milled powders the densification process starts around 300 °C.

Figures 2(b) and 5(b) show the SEM micrographs of fracture surfaces of sintered pellets prepared using sub-micrometric and milled powders, respectively. In the case of sub-micrometric powders, the sintering process emphasizes drastically the lamellar *habitus* of the material. On the other hand, the samples obtained sintering the milled powders (Fig. 5(b)) present a quite uniform microstructure composed by well compacted nanograins, with no indication of anisotropic microstructure.

Figures 7(a and b) report the relative densities of samples sintered in different conditions of temperature and pressure using sub-micrometric (from method A) and

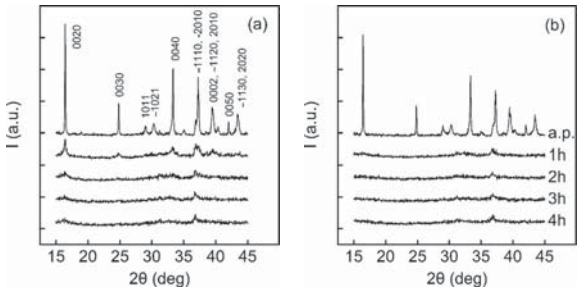

Figure 3. Evolution in the XRD pattern of $Ca_3Co_4O_9$ powder resulting from ball milling of powder "A" at 400 rpm (a) and 600 rpm (b) for different times.

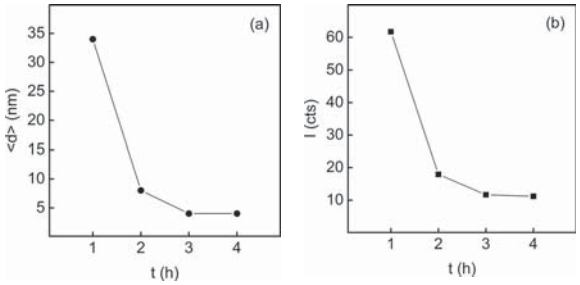

Figure 4. Evolution of grain size (a) and XRD 0020 peak intensity (b) with milling time for $Ca_3Co_4O_9$ powders from method A. Milling speed 400 rpm.

nanometric powders. Samples virtually fully dense, presenting relative densities above 98 vol%, can be obtained using sub-micrometric powders at 750 °C applying a pressure of 180 MPa for 5 min (Fig. 7(a)). Nanometric powders, milled at 400 rpm, can be densified using considerably milder conditions (Fig. 7(b)). The relative density of the samples sintered under a pressure of 180 MPa increases linearly with the sintering temperature, from 76 vol% at 400 °C to 92 vol% at 550 °C. By increasing the pressure to 432 MPa it is possible to obtain a relative density of 98 vol% at 550 °C.

The sintering process, however, produces some recrystallization and grain growth. Figure 8(a) illustrates the differences in the XRD diffraction patterns of milled powders after sintering at temperatures between 400 and 550 °C under a pressure of 180 MPa for 5 min. Up to 450 °C the densification produces a very limited modification in the material, which remains largely amorphous. Starting from 500 °C, a significant increase in peak intensity is observed, although the grain size remains extremely small (see Fig. 8(b)). At 550 °C a crystallite size of 17 nm can be calculated from the FWHM of 0020 peak. The microstructural anisotropy of these samples, however, seems to be quite limited, due to the extremely small grain size.

3.3. Thermoelectric Properties

Figure 9 shows the electrical conductivity of samples obtained from sintering powders prepared using method A, B and milling. For all these samples the electrical

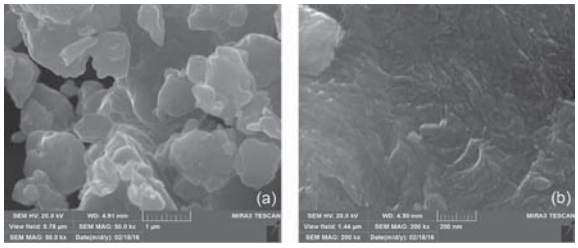

Figure 5. SEM micrographs of milled $Ca_3Co_4O_9$ powder (a) and corresponding sintered sample S09A (b). The ball milling treatment strongly reduces the grain size and leads to a more isotropic morphology.

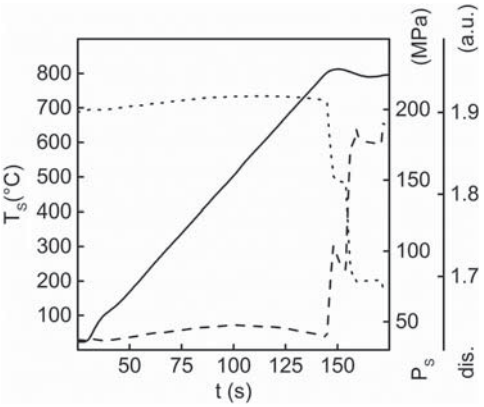

Figure 6. Evolution of temperature (solid), pressure (dash) and displacement (dot) during the HP-FAST sintering of sub-micrometric $Ca_3Co_4O_9$ powders from method A.

conductivity shows little modification in the considered temperature interval. This general trend is similar to the ones reported previously for samples densified using the Spark Plasma Sintering (SPS) technique.[15] The comparison between samples presenting different grain sizes and relative densities allows obtaining some insight on the relative influence of density and grain size on the electrical conductivity. Samples S07A and S08A, for instance, present similar grain size (sub-micrometric, >200 nm), but very different relative densities (94 vol% and 70 vol%, respectively). This increase in porosity produces a moderate decrease in the conductivity.

The influence of grain size, on the other hand, can be deduced comparing the electrical conductivities of two different groups of samples. The first group is represented by samples S07A and S24A. These samples present similar relative densities (94 vol% and 98 vol%, respectively), but extremely different grain size (sub-micrometric >200 nm and 17 nm, respectively). The electrical conductivity appears to be strongly reduced by the nanostructure. A similar behaviour can be observed in another group of samples (S08A, S08B, S09A) presenting similar relative densities (70 vol%, 66 vol% and 76 vol%, respectively),

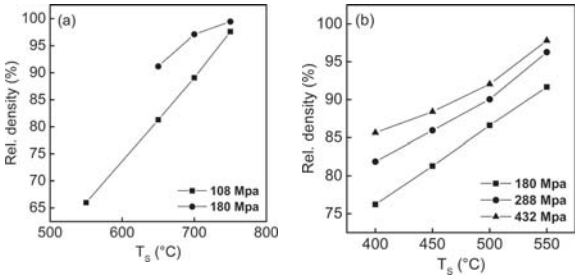

Figure 7. Relative densities of $Ca_3Co_4O_9$ samples obtained using sub-micrometric powders from method A (a) and milled (b) powders sintered under different pressures and temperatures.

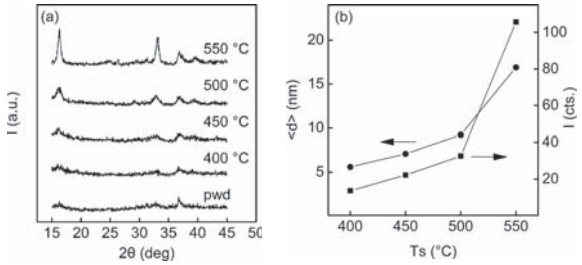

Figure 8. XRD of $Ca_3Co_4O_9$ samples obtained by sintering milled powder at different temperatures (a). Evolution of grain size (circles) and XRD peak intensity (squares) relative to the 0020 peak, as a function of the sintering temperature (b).

but very different grain sizes (sub-micrometric >200 nm, 80 nm, 6 nm, respectively). Also these samples, although being characterized by lower relative density values, show a strong reduction of the electrical conductivity deriving from the reduction of the grain size. These results are not unexpected. It is well known, in fact, that a reduction of the grain size to the nanometric range can produce a significant reduction the electrical conductivity.[16,17] This effect is generally more evident in ceramic materials, particularly when low sintering temperatures are used, and is related to the very large density of grain boundaries present in samples characterized by nanometric grain size.[18]

Figure 10 shows the Seebeck coefficient relative to the same sets of samples described before. The positive sign of the thermopower indicates a *p*-type semiconductor behaviour. It can be seen that Seebeck coefficient increases with temperature, as the electrical conductivity. This behaviour is quite common in this class of materials, as reported by Fergus.[7] Although some differences are observed between the values relative to the samples presenting different density and different grain size, these

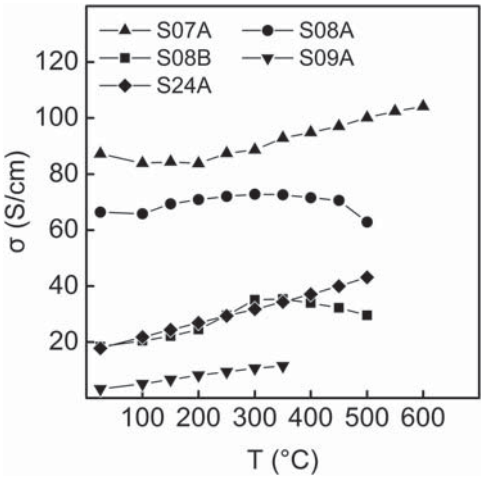

Figure 9. Electrical conductivity of samples S07A (up triangles), S08A (circles), S08B (squares), S09 (down triangles) and S24A (diamonds).

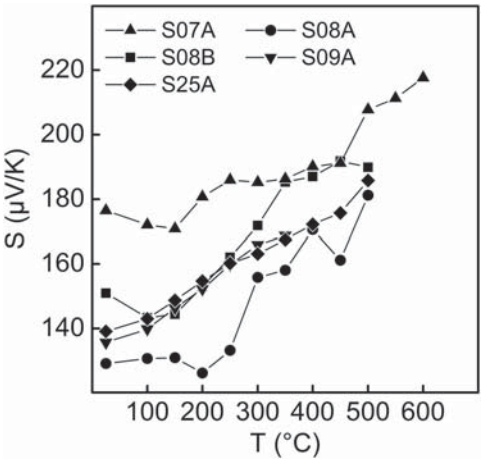

Figure 10. Seebeck coefficient of samples S07A (up triangles), S08A (circles), S08B (squares), S09 (down triangles) and S24A (diamonds).

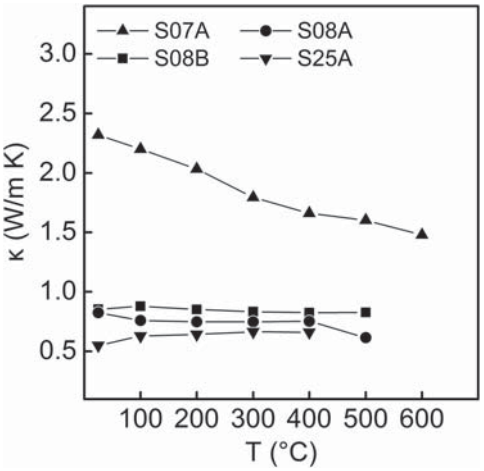

Figure 12. Thermal conductivity of samples S07A (up triangles), S08A (circles), S08B (squares) and sample S25A (down triangles).

differences appear to be quite limited. In particular, the influence of the nanostructure, does not seem to be relevant. In the literature a small increase in the Seebeck coefficient has been sometimes reported in nanostructured materials,[19,20] although no firm physical basis for this increase could be presented.

Figure 11 shows the power factor calculated for the samples S07A, S08A, S08B and S09A. The dependence of the power factor from the relative density and the grain size follows closely the trend shown by the electrical conductivity, as the difference in σ between the various samples is much more relevant than the difference in the Seebeck coefficient. As a result, also in this case the nanostructured samples appear to be less performant. The best power factor presented by samples obtained using milled powders is, in fact, more than two times lower compared to the power factor of the sample characterized by submicrometric grain size.

The thermal conductivities of these samples are reported in Figure 12. Since the laser flash apparatus we used in this investigation can measure only samples with a diameter of 12.7 mm, the thermal conductivity could be determined only on a reduced set of samples, not requiring high pressure for their densification: S07A, S08A, S08B and S25A (the latter can be considered equivalent to sample S09A) (Fig. 12). The thermal conductivities of the samples presenting the lower relative densities (S25A, S08A and S08B, r.d. around 70 vol%) are lower than 1 W/mK and appear to be all quite similar, regardless the grain size. This indicates that in presence of a high level of porosity the role of the grain size appears to be minimized. The only sample presenting high relative density, but also

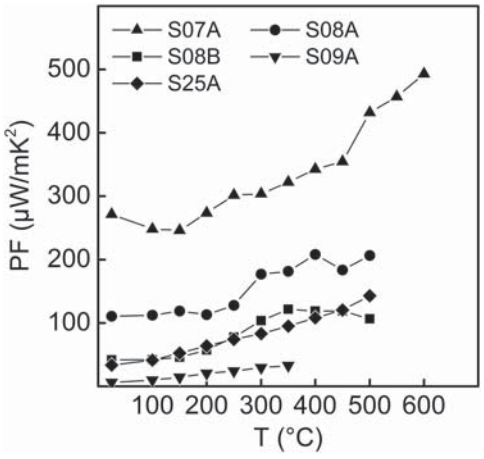

Figure 11. Power factor of samples S07A (up triangles), S08A (circles), S08B (squares), S09 (down triangles) and S24A (diamonds).

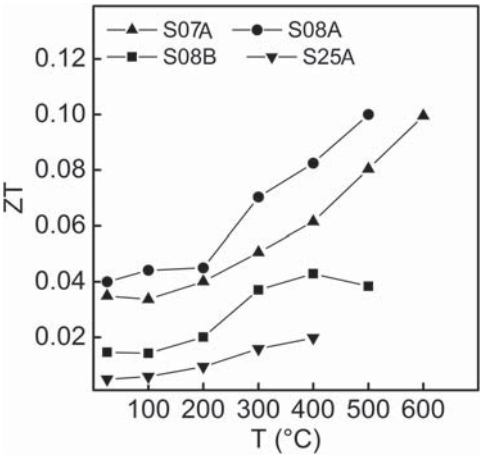

Figure 13. Figure of merit of samples S07A (up triangles), S08A (circles), S08B (squares) and sample S25A (down triangles).

larger grain size (S07A), presents a thermal conductivity that is more than two times higher (2.3 W/m K at RT).

The figure of merit of these sample is reported in Figure 13. These values must be considered only as indicative, due to the large porosity of most samples and to the presence of texturing, particularly in the samples presenting the larger grain size. The electrical conductivity and the thermal conductivity, in fact, have been measured along two mutually perpendicular directions. In any case, the best figure of merit is observed in a sample presenting the larger grain size. This is the result of the drastic reduction in the electrical conductivity observed in the samples presenting the nanometric grain size.

4. CONCLUSIONS

We have demonstrated the possibility of obtaining bulk, dense samples of nanocrystalline $Ca_3Co_4O_9$ using a combination of sol–gel, ball milling and HP-FAST densification. The powders deriving from the solution synthesis presented a lamellar *habitus* characterized by a minimum grain size of 80 nm along the direction parallel to the basal plane. The ball milling produced a strong reduction in the grain size, the disruption of the lamellar microstructure and a general loss of crystallinity. These characteristics could be preserved during the sintering with HP-FAST at temperatures up to 500 °C. Above this temperature some grain growth and recrystallization are observed, although no indication of grain size anisotropy could be observed.

The comparison between the electrical conductivity of samples characterized by similar relative densities but presenting grain sizes spanning more that two order of magnitude, evidenced a significant reduction, strong enough to control the figure of merit of the material. In fact, although the nanostructure produced also some reduction in the thermal conductivity, this resulted to be not large enough to compensate for the decrease in the electrical conductivity. As a result, materials presenting very small grain size and low crystallinity present a figure of merit that is generally inferior than the one shown by materials presenting sub-micrometric grain size.

Acknowledgments: The authors would like to thank I. Quinzeni and P. Mustarelli for the use of the ball milling apparatus. This work has been founded by Fondazione Cariplo under the project "Towards new nanostructured thermoelectric oxides" (grant no. 2012-0815).

References and Notes

1. J. R. Sootsman, D. Y. Chung, and M. G. Kanatzidis, *Angew. Chem. Int. Ed.* 48, 8616 (**2009**).
2. H. Wang, J.-H. Bahk, C. Kang, J. Hwang, K. Kim, J. Kim, P. Burke, J. E. Bowers, A. C. Gossard, A. Shakouri, et al., *Proc. Natl. Acad. Sci.* 111, 10949 **2014**).
3. J. Dong, K. Yang, B. Xu, L. Zhang, Q. Zhang, and Y. Tian, *J. Alloys Compd.* 647, 295 (**2015**).
4. X. Tang, W. Xie, H. Li, W. Zhao, Q. Zhang, and M. Niino, *Appl. Phys. Lett.* 90, 012102 (**2007**).
5. G. Ren, J. Lan, C. Zeng, Y. Liu, B. Zhan, S. Butt, Y.-H. Lin, and C.-W. Nan, *JOM* 67, 211 (**2015**).
6. A. Sotelo, G. Constantinescu, S. Rasekh, M. A. Torres, J. C. Diez, and M. A. Madre, *J. Eur. Ceram. Soc.* 32, 2415 (**2012**).
7. J. W. Fergus, *J. Eur. Ceram. Soc.* 32, 525 (**2012**).
8. Y. Miyazaki, M. Onoda, T. Oku, M. Kikuchi, Y. Ishii, Y. Ono, Y. Morii, and T. Kajitani, *J. Phys. Soc. Jpn.* 71, 491 (**2002**).
9. K. Obata, Y. Chonan, T. Komiyama, T. Aoyama, H. Yamaguchi, and S. Sugiyama, *J. Electron. Mater.* 42, 2221 (**2013**).
10. K. Biswas, J. He, I. D. Blum, C.-I. Wu, T. P. Hogan, D. N. Seidman, V. P. Dravid, and M. G. Kanatzidis, *Nature* 489, 414 (**2012**).
11. D.-W. Kim, Y.-D. Ko, J.-G. Park, and B.-K. Kim, *Angew. Chem. Int. Ed.* 46, 6654 (**2007**).
12. F. Maglia, I. G. Tredici, and U. Anselmi-Tamburini, *J. Eur. Ceram. Soc.* 33, 1045 (**2013**).
13. Y. C. Liou, W. C. Tsai, W. Y. Lin, and U. R. Lee, *J. Aust. Ceram. Soc.* 44, 17 (**2008**).
14. D. Sedmidubský, V. Jakeš, O. Jankovský, J. Leitner, Z. Sofer, and J. Hejtmánek, *J. Solid State Chem.* 194, 199 (**2012**).
15. Y. Liu, Y. Lin, Z. Shi, C.-W. Nan, and Z. Shen, *J. Am. Ceram. Soc.* 88, 1337 (**2005**).
16. X. Guo, *Scr. Mater.* 65, 96 (**2011**).
17. X. Guo and Z. Zhang, *Acta Mater.* 51, 2539 (**2003**).
18. U. Anselmi-Tamburini, J. E. Garay, Z. A. Munir, A. Tacca, F. Maglia, G. Chiodelli, and G. Spinolo, *J. Mater. Res.* 19, 3263 (**2004**).
19. J.-F. Li, W.-S. Liu, L.-D. Zhao, and M. Zhou, *NPG Asia Mater.* 2, 152 (**2010**).
20. H. Ohta, S. Kim, Y. Mune, T. Mizoguchi, K. Nomura, S. Ohta, T. Nomura, Y. Nakanishi, Y. Ikuhara, M. Hirano, H. Hosono, and K. Koumoto, *Nat. Mater.* 6, 129 (**2007**).

Received: 14 March 2016. Accepted: 27 June 2016.